INTERNATIONAL JOURNAL FOR NUMERICAL METHODS IN FLUIDS
Int. J. Numer. Meth. Fluids 2000; **32**: 465–493

A numerical method for the evaluation of hydrodynamic forces of translating bodies under a free surface

S.A. Yang*

Department of Naval Architecture and Marine Engineering, National Cheng Kung University, Tainan, Taiwan, ROC

SUMMARY

This paper presents a numerical method to evaluate the hydrodynamic forces of translating bodies under a free surface. Both steady and unsteady problems are considered. Analytical and numerical studies are carried out based on the Havelock wave-source function and the integral equation method. Two main problems arising inherently in the proposed solution method are overcome in order to facilitate the numerical implementation. The first lies in evaluating the Havelock function, which involves integrals with highly oscillatory kernels. Particular integration contours leading to non-oscillatory integrands are derived *a priori* so that the integrals can be evaluated efficiently. The second problem lies in evaluating singular kernels in the boundary integral equation. The corresponding non-singular formulation is derived using some theorems of potential theory, including the Gauss flux theorem and the property related to the equipotential body. The subsequent formulation is amenable to the solution by directly using the standard quadrature formulas without taking another special treatment. This paper also attempts to enhance the computational efficiency by presenting an interpolation method used to evaluate matrix elements, which are ascribed to a discretization procedure. In addition to the steady case, numerical examples consist of cases involving a submerged prolate spheroid, which is originally idle and then suddenly moves with a constant speed and a constant acceleration. Also systematically studied is the variation of hydrodynamic forces acting on the spheroid for various Froude numbers and submergence depths. Copyright © 2000 John Wiley & Sons, Ltd.

KEY WORDS: potential flow; free surface problem; Havelock wave-source function; integral equation method; desingularization

1. INTRODUCTION

On the basis of the linearized theory of water waves, the complete velocity potential ϕ for the three-dimensional (3D) flow of a previously undisturbed fluid with a uniform stream of velocity $-u(t)$ parallel to the x-axis past a point source $\sigma_0(t)$ at point $q(\xi, \eta, \zeta)$ can be expressed as

* Correspondence to: Department of Naval Architecture and Marine Engineering, National Cheng Kung University, Tainan, Taiwan 70101, ROC.

CCC 0271–2091/2000/040465–29$17.50

Received July 1998
Revised January 1999

$$\phi = -u(t)x + \varphi(x, y, z; t), \tag{1}$$

where t denotes the time and φ represents the disturbed velocity potential. A right-handed rectangular co-ordinate system is chosen with the origin located at the level of the undisturbed free surface and the y-axis vertically upwards. The Green function, commonly referred to as the Havelock wave-source function, can be written in a conventional form as [1]

$$\begin{aligned}&\varphi(x, y, z; t)\\ &= -\frac{\sigma_0(t)}{r_1} + \frac{\sigma_0(t)}{r_2} - \frac{g^{1/2}}{\pi}\int_0^t \sigma_0(\tau)\,\mathrm{d}\tau \int_{-\pi}^{\pi} \mathrm{d}\theta \int_0^{\infty} k^{1/2}\,\mathrm{d}k\, \sin[(kg)^{1/2}(t-\tau)]\\ &\quad \times \exp\left\{k(y+\eta) + ik\left[(x-\xi) + \int_\tau^t u(\tau)\,\mathrm{d}\tau\right]\cos\theta + ik(z-\zeta)\sin\theta\right\},\end{aligned} \tag{2}$$

where

$$r_1 = [(x-\xi)^2 + (y-\eta)^2 + (z-\zeta)^2]^{1/2},$$

$$r_2 = [(x-\xi)^2 + (y+\eta)^2 + (z-\zeta)^2]^{1/2},$$

i denotes the imaginary unit, g represents the acceleration of gravity, and $\sigma_0(t) = 0$ when $t < 0$. Introducing the integral equation (IE) method combined with Equations (1) and (2) allows us to reduce the problem and, ultimately, to determine the source strengths on the body surface. Obviously, the crux of the numerical implementation depends on accurately evaluating the integral in Equation (2).

Most studies relating to the unsteady problem have focused on the approximation methods. Sretenskii [2] first derived an expression of the wave resistance for a thin ship in non-uniform motion. Havelock [3,4] used the method of stationary phase to obtain the asymptotic expansions of solution. Wehausen [5] dealt with a problem resembling that of Havelock [3,4] by applying the theory of Fourier integrals toward large time and small time. Shebalov [6] applied the method of series expansion to the corresponding non-linear problem. Through asymptotic analyses, Liu and Yue [7] studied the unsteady behavior of the solution at large time. Previous works generally indicate that the wave resistance of a body with an impulsive or gradual start displays an oscillating and slowly decaying behavior. However, results obtained from the approximation methods are available only for the large and small values of a chosen parameter. If the continuously varying dynamic effects from the beginning of motion are of interest, the use of numerical methods may be virtually indispensable. Under this circumstance, evaluating the integral of the highly oscillatory function involved in Equation (2) is relatively difficult. Smith *et al.* [8] and Shen and Farell [9] studied a steady state case of Equation (2), i.e. $t \to \infty$. The principal value integral was transformed into an integral along a particular integration contour in the complex plane, thereby eliminating the oscillatory behavior. Newman [10] approximated the double integral in terms of 3D polynomials.

In light of the above developments, this paper presents a numerical method to investigate the hydrodynamic forces acting on a translating body under a free surface. The

Havelock-source method and the IE method form the framework of the solution algorithm. The IE method is a conventional approach to the exterior problems. This approach is highly attractive owing to its ability not only to reduce the dimensionality of the problem by one, but also to transform an infinite domain to finite boundaries in which the far-field (radiation) condition is automatically satisfied. From a numerical perspective, both of these features are crucial. Three different types of singularities generally appear in the integral equation formulation: weak singularity, Cauchy principal value singularity and hypersingularity. The handling of the singular integrals has received extensive attention, as have the numerous techniques proposed. Huang and Cruse [11] classified these techniques into the following categories: analytical method; semi-analytical method; degenerate mapping and rigid body movement method; special Gaussian type method; modified boundary integral equation; and finite-part method. Selecting which method to adopt encompasses issues of problem dependence and personal preference dependence. Landweber and Macagno [12] developed an effective means of transforming the integral equation to a non-singular form using some properties of potential theory.

The remainder of the paper is organized as follows. Section 2 describes the integral equation formulation and the extension of Landweber and Macagno's [12] method to the current problem. The Green function defined by Equation (2), which takes into account the free surface effect, is adopted herein; the oscillatory behavior of the integral is also alleviated by extending Shen and Farell's [9] method. The reason of adopting this approach is ascribed to the fact that the contour integration method can be conveniently extended to the unsteady problem. Section 3 presents the details of deriving integration contours. Results obtained from the IE methods indicate that a substantial amount of computation time is generally expended on evaluating the matrix elements, not on the solution to the system of simultaneous linear algebraic equations itself. Notably, the numerical computation becomes extremely difficult when an unsteady problem is of primary concern. Section 4 describes a simple interpolation method capable of enhancing the computational efficiency. The efficacy of the proposed solution method is justified in Section 5 by comparing the calculations with the available analytical solutions. Also systematically studied herein are the physical cases of a translating prolate spheroid under a free surface by varying the Froude number and the submergence depth. Section 6 concludes this paper.

2. INTEGRAL EQUATION FORMULATION

This section mathematically formulates the IE method and the regularization method of singular kernels. Consider a uniform flow with velocity $u(t)$ in the direction of the negative x-axis past a stationary, submerged body with the boundary surface ∂B of Lyapunov type. The fluid is assumed to be inviscid and incompressible. The Lyapunov surfaces are defined in Günter [13]. A Lyapunov surface, although having a continuously varying tangent plane at each point, does not necessarily possess a curvature everywhere. In terms of the Bernoulli equation

$$\frac{P}{\rho}+\frac{1}{2}\nabla\phi\cdot\nabla\phi+\frac{\partial\varphi}{\partial t}-\frac{1}{2}u^2=\text{constant}, \tag{3}$$

the jth force acting on the body can be written as

$$F_j = -\int_{\partial B} Pn_j \, \mathrm{d}S = \rho \int_{\partial B} \left(\frac{\partial \varphi}{\partial t} + \frac{1}{2} \nabla\phi \cdot \nabla\phi \right) n_j \, \mathrm{d}S, \tag{4}$$

where P and ρ denote the pressure and the density of the fluid respectively, and n_j represents the jth component of the outward normal on the body surface.

Initially, consider the term $\partial\varphi/\partial t$ involved in Equation (4). By making use of Equations (1) and (2), a continuous distribution of sources σ over ∂B generates the single-layer potential at point p in the following form:

$$\phi_p = -ux - \int_{\partial B} \frac{\sigma_q}{r_1} \, \mathrm{d}S_q + \int_{\partial B} \frac{\sigma_q}{r_2} \, \mathrm{d}S_q - \int_{\partial B} G \, \mathrm{d}S_q, \tag{5}$$

where $p(x, y, z)$ and $q(\xi, \eta, \zeta)$ denote the field and source points respectively, σ_q denotes the source density at q, and G represents the third term on the right-hand side of Equation (2). According to Equations (2) and (5), $\partial\varphi/\partial t$ can be expressed as

$$\frac{\partial \varphi_p}{\partial t} = -\int_{\partial B} \frac{1}{r_1} \frac{\partial \sigma_q}{\partial t} \, \mathrm{d}S_q + \int_{\partial B} \frac{1}{r_2} \frac{\partial \sigma_q}{\partial t} \, \mathrm{d}S_q - \int_{\partial B} \frac{\partial G}{\partial t} \, \mathrm{d}S_q. \tag{6}$$

Notably, a singularity arises in the first integral of the preceding equation when $r_1 \to 0$.

To remove the singular behavior, Equation (6) is rewritten as follows:

$$\begin{aligned} \frac{\partial \varphi_p}{\partial t} &= -\int_{\partial B} \frac{1}{r_1} \left(\frac{\partial \sigma_q}{\partial t} - \frac{\partial \sigma_p}{\partial t} \frac{\sigma_q^*}{\sigma_p^*} \right) \mathrm{d}S_q - \frac{\partial \sigma_p}{\partial t} \frac{1}{\sigma_p^*} \int_{\partial B} \frac{1}{r_1} \sigma_q^* \, \mathrm{d}S_q + \int_{\partial B} \frac{1}{r_2} \frac{\partial \sigma_q}{\partial t} \, \mathrm{d}S_q - \int_{\partial B} \frac{\partial G}{\partial t} \, \mathrm{d}S_q \\ &= -\int_{\partial B} \frac{1}{r_1} \left(\frac{\partial \sigma_q}{\partial t} - \frac{\partial \sigma_p}{\partial t} \frac{\sigma_q^*}{\sigma_p^*} \right) \mathrm{d}S_q + \frac{\partial \sigma_p}{\partial t} \frac{\phi_e}{\sigma_p^*} + \int_{\partial B} \frac{1}{r_2} \frac{\partial \sigma_q}{\partial t} \, \mathrm{d}S_q - \int_{\partial B} \frac{\partial G}{\partial t} \, \mathrm{d}S_q, \end{aligned} \tag{7}$$

where σ^* is a source distribution on ∂B and makes the surface an equipotential of potential ϕ_e, which is defined by

$$\phi_e = -\int_{\partial B} \frac{1}{r_1} \sigma_q^* \, \mathrm{d}S_q. \tag{8}$$

Landweber and Macagno [12] proved that the first integrand of Equation (7) can be set equal to zero when $r_1 \to 0$. Thus, Equation (7) represents the non-singular form of Equation (6) and can be implemented numerically by directly using standard quadrature formulas.

Next, consider the formulation of the source density σ^* involved in Equation (7). The velocity in the interior domain of an equipotential body vanishes and, therefore, the source density σ^* can be expressed as follows:

$$2\pi\sigma_p^* = -\int_{\partial B} \sigma_q^* \frac{\partial}{\partial n_p}\left(\frac{1}{r_1}\right) \mathrm{d}S_q, \tag{9}$$

where $\partial/\partial n_p$ denotes differentiation in the outward normal direction at point p on the body surface. This equation is also inhibited by the appearance of singular kernel when $r_1 \to 0$. The kernel in Equation (9) is weakly singular because, for a Lyapunov surface, it is of order $1/r_1^{N-L}$ with $0 < L \leq 1$, where L denotes the Lyapunov exponent [14]. Equation (9) can be rewritten in the following form:

$$2\pi\sigma_p^* = -\int_{\partial B} \left[\sigma_q^* \frac{\partial}{\partial n_p}\left(\frac{1}{r_1}\right) - \sigma_p^* \frac{\partial}{\partial n_q}\left(\frac{1}{r_1}\right)\right] \mathrm{d}S_q - \sigma_p^* \int_{\partial B} \frac{\partial}{\partial n_q}\left(\frac{1}{r_1}\right) \mathrm{d}S_q. \tag{10}$$

By applying the Gauss flux theorem,

$$\int_{\partial B} \frac{\partial}{\partial n_q}\left(\frac{1}{r_1}\right) \mathrm{d}S_q = -2\pi, \tag{11}$$

Equation (10) reduces to

$$0 = \int_{\partial B} \left[\sigma_q^* \frac{\partial}{\partial n_p}\left(\frac{1}{r_1}\right) - \sigma_p^* \frac{\partial}{\partial n_q}\left(\frac{1}{r_1}\right)\right] \mathrm{d}S_q, \tag{12}$$

in which the integrand can be set equal to zero as $r_1 \to 0$. Notably, Equation (12) yields infinite families of unknown function σ^*. This problem, however, causes no difficulty in numerical implementation by assigning a value of σ^* at a chosen point. The unknown constant is automatically factored out, as can be seen in Equation (7). After σ^* is solved by Equation (12), the corresponding velocity potential ϕ_e can be straightforwardly obtained through Equation (8). The fact that ϕ_e remains constant in the interior of an equipotential surface accounts for the reason why its value can be computed conveniently by locating point p inside the boundary surface. This trick then avoids a situation in which q coincides with p.

The time derivative of source function σ involved in Equation (7) must also be evaluated to determine $\partial\varphi/\partial t$. Initially, consider the source function σ itself. By applying the no-penetration condition over the impermeable boundary, we have, from Equation (5),

$$0 = 2\pi\sigma_p - u\frac{\partial x}{\partial n_p} - \int_{\partial B} \sigma_q \frac{\partial}{\partial n_p}\left(\frac{1}{r_1}\right) \mathrm{d}S_q + \int_{\partial B} \sigma_q \frac{\partial}{\partial n_p}\left(\frac{1}{r_2}\right) \mathrm{d}S_q - \int_{\partial B} \frac{\partial G}{\partial n_p} \mathrm{d}S_q. \tag{13}$$

Notably, the first integral in Equation (13) possesses a singularity when $r_1 \to 0$. Again, the difficulty can be avoided by subtracting a function from the integrand and adding it back with an exact value. Thus, Equation (13) can be rewritten as

$$0 = 2\pi\sigma_p - u\frac{\partial x}{\partial n_p} - \int_{\partial B}\left[\sigma_q \frac{\partial}{\partial n_p}\left(\frac{1}{r_1}\right) - \sigma_p \frac{\partial}{\partial n_q}\left(\frac{1}{r_1}\right)\right] S_q - \sigma_p \int_{\partial B} \frac{\partial}{\partial n_q}\left(\frac{1}{r_1}\right) \mathrm{d}S_q + \int_{\partial B} \sigma_q \frac{\partial}{\partial n_p}\left(\frac{1}{r_2}\right) \mathrm{d}S_q - \int_{\partial B} \frac{\partial G}{\partial n_p}\, \mathrm{d}S_q. \tag{14}$$

Substituting the Gauss flux theorem (11) into the above equation leads to

$$0 = 4\pi\sigma_p - u\frac{\partial x}{\partial n_p} - \int_{\partial B}\left[\sigma_q \frac{\partial}{\partial n_p}\left(\frac{1}{r_1}\right) - \sigma_p \frac{\partial}{\partial n_q}\left(\frac{1}{r_1}\right)\right] \mathrm{d}S_q + \int_{\partial B} \sigma_q \frac{\partial}{\partial n_p}\left(\frac{1}{r_2}\right) \mathrm{d}S_q - \int_{\partial B} \frac{\partial G}{\partial n_p}\, \mathrm{d}S_q. \tag{15}$$

The subsequent integrand of the first integral in this equation can be numerically set equal to zero when $r_1 \to 0$. From Equation (15), the non-singular form of the time derivative of σ can be written as

$$0 = 4\pi \frac{\partial \sigma_p}{\partial t} - \frac{\partial u}{\partial t}\frac{\partial x}{\partial n_p} - \int_{\partial B}\left[\frac{\partial \sigma_q}{\partial t}\frac{\partial}{\partial n_p}\left(\frac{1}{r_1}\right) - \frac{\partial \sigma_p}{\partial t}\frac{\partial}{\partial n_q}\left(\frac{1}{r_1}\right)\right] \mathrm{d}S_q + \int_{\partial B} \frac{\partial \sigma_q}{\partial t}\frac{\partial}{\partial n_p}\left(\frac{1}{r_2}\right) \mathrm{d}S_q - \int_{\partial B} \frac{\partial^2 G}{\partial t\, \partial n_p}\, \mathrm{d}S_q. \tag{16}$$

Until now, we have demonstrated that the term $\partial\varphi/\partial t$ in Equation (4) can be obtained from Equation (7) after σ^*, ϕ_e and $\partial\sigma/\partial t$ are solved from Equations (12), (8) and (16) respectively. These equations are striking in that they are all in non-singular form and, therefore, are conducive to numerical implementation. Equation (16) is a Fredholm integral equation of the second kind and is solved by an iterative method given in Section 5. Equation (12) can also be categorized as a Fredholm integral equation of the second kind by viewing its original form in Equation (9). In doing so, the same iterative method can be used.

Next, consider the term $\nabla\phi$ in Equation (4). Provided that the surface source distribution is Hölder continuous, the tangential derivatives of ϕ exist and are continuous [15]. Thus, the tangential velocity $u_s^{(j)}$ along the $\xi^{(j)}$-axis at point p on the body surface takes the following form:

$$u_s^{(j)} = \frac{1}{h^{(j)}}\frac{\partial \phi}{\partial \xi_p^{(j)}}, \tag{17}$$

where $h^{(j)}$ denotes the corresponding scale factor, $j = 1, 2$, and

$$\frac{\partial \phi}{\partial \xi_p^{(j)}} = -u\frac{\partial x}{\partial \xi_p^{(j)}} - \int_{\partial B} \sigma_q \frac{\partial}{\partial \xi_p^{(j)}}\left(\frac{1}{r_1}\right) \mathrm{d}S_q + \int_{\partial B} \sigma_q \frac{\partial}{\partial \xi_p^{(j)}}\left(\frac{1}{r_2}\right) \mathrm{d}S_q - \int_{\partial B} \frac{\partial G}{\partial \xi_p^{(j)}}\, \mathrm{d}S_q, \tag{18}$$

provided that the first integral is interpreted in the sense of the Cauchy principal value [16,17]. Correspondingly, the velocity components in the Cartesian co-ordinates xyz, or for convenience $x^{(1)}x^{(2)}x^{(3)}$, can be expressed as follows:

$$u^{(j)} = \frac{\partial \phi}{\partial x_P^{(j)}} = -u\delta_{j,1} + 2\pi\sigma_P n_j - \int_{\partial B} \sigma_q \frac{\partial}{\partial x_P^{(j)}}\left(\frac{1}{r_1}\right) \mathrm{d}S_q + \int_{\partial B} \sigma_q \frac{\partial}{\partial x_P^{(j)}}\left(\frac{1}{r_2}\right) \mathrm{d}S_q - \int_{\partial B} \frac{\partial G}{\partial x_p^{(j)}} \mathrm{d}S_q, \tag{19}$$

where $j = 1, 2, 3$ and $\delta_{j,1}$ represents the Kronecker delta. The Cauchy principal value integral in Equation (19) is evaluated by a simple and efficient quadrature formula described in Section 5.

3. TREATMENT OF THE OSCILLATORY INTEGRALS

The integrand in Equation (2) is highly oscillatory at a large k. This fact implies that the numerical implementation is rather difficult. This section presents an effective means of dealing with this oscillatory integral. Other alternative approaches to this problem (e.g. [18–20]) have been proposed. However, the method presented in this section appears to be more appropriate for the type of integral given in Equation (2).

Function G, defined as the third term on the right-hand side of Equation (2), is quite general. For instance, for an impulsive motion with constant velocity $-u_c$ and a source with constant strength σ_c, G reduces to

$$G\Big|_{\sigma=\sigma_c}^{u=u_c} = -\frac{4\sigma_c k_c}{\pi} \int_0^{\pi/2} \sec^2\theta \, \mathrm{d}\theta \int_0^{\infty} \frac{\cos[k(x-\xi)\cos\theta]\cos[k(z-\zeta)\sin\theta]}{k - k_c \sec^2\theta} \times \exp[k(y+\eta)]\,\mathrm{d}k + \frac{g^{1/2}\sigma_c}{\pi u_c^2} \int_0^{\pi/2} \sec^2\theta \, \mathrm{d}\theta \int_0^{\infty} \mathrm{d}k \exp\{k(y+\eta) + ik[(x-\xi)\cos\theta \pm (z-\zeta)\sin\theta]\} \times \frac{[ku_c\cos\theta + (gk)^{1/2}]\exp\{it[ku_c\cos\theta - (gk)^{1/2}]\} - [ku_c\cos\theta - (gk)^{1/2}]\exp\{it[ku_c\cos\theta + (gk)^{1/2}]\}}{k^{1/2}(k - k_c\sec^2\theta)}, \tag{20}$$

which is a sum of time-dependent and time-independent terms, and $k_c = g/u_c^2$. In addition, the $\pm$ signs in Equation (20) indicate that the contributions of the minus and plus signs should be calculated separately and added. Furthermore, when $t \to \infty$, Equation (20) reduces to

$$\lim_{t\to\infty} G\Big|_{\sigma=\sigma_c}^{u=u_c} = -\frac{4\sigma_c k_c}{\pi} \int_0^{\pi/2} \sec^2\theta \, \mathrm{d}\theta \int_0^{\infty} \frac{\cos[k(x-\xi)\cos\theta]\cos[k(z-\zeta)\sin\theta]}{k - k_c\sec^2\theta} \times \exp[k(y+\eta)]\,\mathrm{d}k - 4k_c\sigma_c \int_0^{\pi/2} \sec^2\theta \sin[k_c(x-\xi)\sec\theta] \times \cos[k_c(z-\zeta)\sec^2\theta\sin\theta] \times \exp[k_c(y+\eta)\sec^2\theta]\,\mathrm{d}\theta. \tag{21}$$

The mathematical derivations of Equations (20) and (21) are well known, although not straightforward in manipulation; therefore, they are not repeated herein. However, these two cases serve as the test examples in Section 5.

To study the oscillatory behavior of function G, let us first approximate it by

$$G \approx \sum_{n=1}^{N} G_n = \sum_{n=1}^{N} \sigma_n \int_{t_{n-1}}^{t_n} f(\tau)\, \mathrm{d}\tau, \tag{22}$$

where

$$\begin{aligned}\int_{t_{n-1}}^{t_n} f(\tau)\, \mathrm{d}\tau = \frac{g^{1/2}}{\pi u_n^2} \int_0^{\pi/2} \sec^2\theta\, \mathrm{d}\theta \int_0^{\infty} \mathrm{d}k\, \exp\{k(y+\eta) + ik[(x-\xi)\cos\theta \pm (z-\zeta)\sin\theta]\} \\ \times \frac{[ku_n\cos\theta + (gk)^{1/2}]\exp\{iT[ku_n\cos\theta - (gk)^{1/2}]\} - [ku_n\cos\theta - (gk)^{1/2}]\exp\{iT[ku_n\cos\theta + (gk)^{1/2}]\}}{k^{1/2}(k - k_n\sec^2\theta)} \Bigg|_{T=t-t_n}^{T=t-t_{n-1}} \\ \equiv F_n(x-\xi, y+\eta, z-\zeta; T)\big|_{T=t-t_n}^{T=t-t_{n-1}},\end{aligned} \tag{23}$$

where $k_n = g/u_n^2$, $t_0 = 0$, and $t_N = t$. In Equation (22), the source strength σ_n and velocity u_n in each time step are assumed to remain constant. The integrand in Equation (23) is highly oscillatory at a large k owing to the imaginary argument of the exponential function, in which k appears as a factor. For convenience, define

$$\begin{aligned}I_n = \int_0^{\infty} \frac{[ku_n\cos\theta + (gk)^{1/2}]\exp\{iT[ku_n\cos\theta - (gk)^{1/2}]\} - [ku_n\cos\theta - (gk)^{1/2}]\exp\{iT[ku_n\cos\theta + (gk)^{1/2}]\}}{k^{1/2}(k - k_n\sec^2\theta)} \\ \times \exp[k(y+\eta) + ik\omega]\, \mathrm{d}k,\end{aligned} \tag{24}$$

where $\omega = (x-\xi)\cos\theta \pm (z-\zeta)\sin\theta$. Let $\alpha = k^{1/2}$; then, we have a situation in which $I_n = I_{n,1} + I_{n,2}$, where

$$\begin{aligned}I_{n,1} &= 2\int_0^{\infty} \frac{(\alpha^2 u_n\cos\theta + \alpha g^{1/2})\exp[iT(\alpha^2 u_n\cos\theta - \alpha g^{1/2})]}{\alpha^2 - k_n\sec^2\theta} \exp[\alpha^2(y+\eta) + i\alpha^2\omega]\, \mathrm{d}\alpha \\ &\equiv \int_0^{\infty} f_{n,1}(\alpha)\, \mathrm{d}\alpha,\end{aligned} \tag{25}$$

$$I_{n,2} = 2\int_0^{\infty} \frac{\alpha u_n\cos\theta\exp[iT(\alpha^2 u_n\cos\theta + \alpha g^{1/2}) + \alpha^2(y+\eta) + i\alpha^2\omega]}{\alpha + k_n^{1/2}\sec\theta}\, \mathrm{d}\alpha \equiv \int_0^{\infty} f_{n,2}(a)\, \mathrm{d}\alpha. \tag{26}$$

Notably, $I_{n,1}$ is a Cauchy principal value integral and $I_{n,2}$ is a regular integral. In the complex plane $c = \alpha + i\beta$, the real and imaginary arguments of the exponential function involved in $f_{n,1}(c)$ are given by

$$A_{re} = (\alpha^2 - \beta^2)(y + \eta) - 2\alpha\beta(\omega + u_n T \cos\theta) + g^{1/2}\beta T \tag{27}$$

and

$$A_{im} = 2\alpha\beta(y + \eta) + (\alpha^2 - \beta^2)(\omega + u_n T \cos\theta) - g^{1/2}\alpha T \tag{28}$$

respectively. Figure 1 depicts a typical integration contour. To alleviate the oscillatory behavior, the condition $A_{im} = 0$ must be applied along Path 4. Also required herein is that

$$\lim_{\alpha \to \infty} A_{re} \to -\infty,$$

in order to ensure the convergence of integration. When $\omega + u_n T \cos\theta \neq 0$, it follows that

$$\left(\frac{\beta}{\alpha}\right)^2 - 2\frac{\beta}{\alpha}\left(Q - \frac{g^{1/2}T}{2\alpha|y + \eta|}\right) - 1 < 0 \tag{29}$$

and

$$\left(\frac{\beta}{\alpha} + \frac{1}{Q}\right)^2 = 1 + \frac{1}{Q^2} - \frac{g^{1/2}T}{Q\alpha|y + \eta|}, \tag{30}$$

where Q is defined by

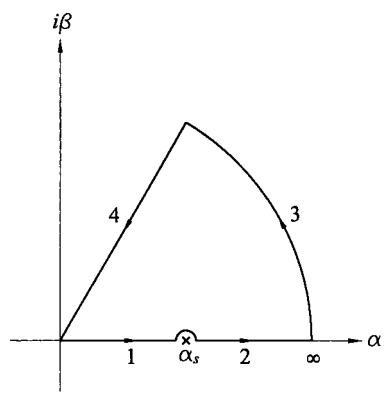

Figure 1. Typical contour of integration in the complex plane $c = \alpha + i\beta$. 'α_s' denotes a singular point.

$$Q = \frac{\omega + u_n T \cos\theta}{|y+\eta|}. \tag{31}$$

Solving Equations (29) and (30) for β yields

$$-\left[\alpha^2 + \left(Q\alpha - \frac{g^{1/2}T}{2|y+\eta|}\right)^2\right]^{1/2} + \left(Q\alpha - \frac{g^{1/2}T}{2|y+\eta|}\right) < \beta$$
$$< \left[\alpha^2 + \left(Q\alpha - \frac{g^{1/2}T}{2|y+\eta|}\right)^2\right]^{1/2} + \left(Q\alpha - \frac{g^{1/2}T}{2|y+\eta|}\right) \tag{32}$$

and

$$\beta = \pm\left[\alpha^2\left(1+\frac{1}{Q^2}\right) - \alpha\frac{g^{1/2}T}{Q|y+\eta|}\right]^{1/2} - \frac{\alpha}{Q} \equiv \pm P_1 - \frac{\alpha}{Q} \tag{33}$$

respectively. Obviously, values in the square brackets of Equation (33) should always remain non-negative. In addition, the values of β should always contain the same positive or negative sign, i.e. the integration contour can not pass through the real axis. Hence, we have

$$\beta = P_1 - \frac{\alpha}{Q}, \quad \alpha \geq \frac{g^{1/2}T}{Q|y+\eta|}, \quad \text{for } Q > 0 \tag{34}$$

and

$$\beta = -P_1 - \frac{\alpha}{Q}, \quad \alpha \geq 0, \quad \text{for } Q < 0. \tag{35}$$

From Equations (27) and (28), we have

$$\beta = -\frac{g^{1/2}T}{2|y+\eta|}, \quad \alpha \geq 0, \quad \text{for } Q = 0. \tag{36}$$

Depending on the values of Q, the original oscillatory behavior can be alleviated by integrating along the contours (Figure 2) governed by Equations (34)–(36) respectively. As Figure 2 depicts, α_1^* is defined by $g^{1/2}T/(Q|y+\eta|)$ and α_s is a singular point defined by $k_n^{1/2}\sec\theta$. Consequently, with the assistance of the residue integration method, the original integral $I_{n,1}$ is transformed to

$$I_{n,1} = I_1 - I_4 + \pi i \operatorname*{Res}_{\alpha=\alpha_s} f_{n,1}(c), \quad \text{for } Q > 0 \text{ and } \alpha_s > \alpha_1^*, \tag{37}$$

$$I_{n,1} = I_1 - I_4, \quad \text{for } Q > 0 \text{ and } \alpha_s < \alpha_1^*, \tag{38}$$

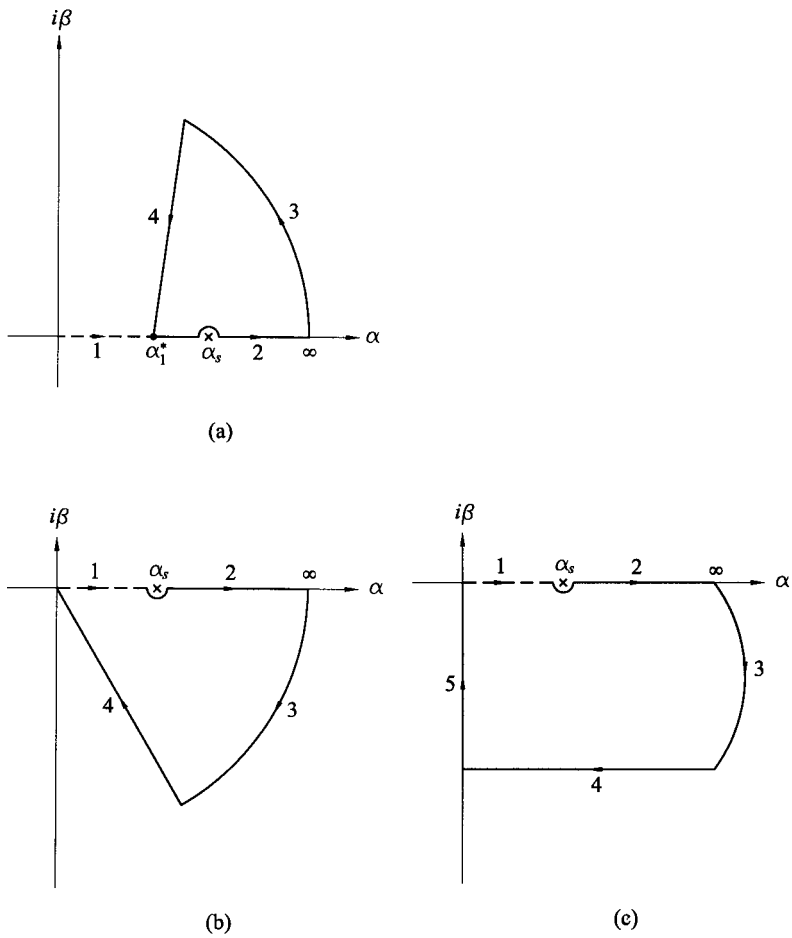

Figure 2. Contour of integration in the complex plane for $I_{n,1}$ with (a) $Q>0$, (b) $Q<0$, and (c) $Q=0$.

$$I_{n,1} = -I_4 - \pi i \operatorname*{Res}_{\alpha=\alpha_s} f_{n,1}(c), \quad \text{for } Q<0 \tag{39}$$

and

$$I_{n,1} = -I_4 - I_5 - \pi i \operatorname*{Res}_{\alpha=\alpha_s} f_{n,1}(c), \quad \text{for } Q=0, \tag{40}$$

where I_j denotes the integration along Path j. Notably, all of the integrals on the right-hand side of Equations (37)–(40) are regular with one exception, in which I_1 in Equation (38) is a Cauchy principal value integral.

Proceeding as before, the integration contours for Equation (26) can be obtained as follows:

$$\beta = P_2 - \frac{\alpha}{Q}, \quad \alpha \geq 0, \quad \text{for } Q > 0, \tag{41}$$

$$\beta = -P_2 - \frac{\alpha}{Q}, \quad \alpha \geq -\frac{g^{1/2}T}{Q|y+\eta|}, \quad \text{for } Q < 0 \tag{42}$$

and

$$\beta = \frac{g^{1/2}T}{2|y+\eta|}, \quad \alpha \geq 0, \quad \text{for } Q = 0, \tag{43}$$

where

$$P_2 = \left[\alpha^2\left(1 + \frac{1}{Q^2}\right) + \alpha\frac{g^{1/2}T}{Q|y+\eta|}\right]^{1/2}. \tag{44}$$

Figure 3 displays the corresponding integration contour for each case, where α_2^* is defined by $-g^{1/2}T/(Q|y+\eta|)$. Correspondingly, the original integral $I_{n,2}$ is transformed to

$$I_{n,2} = -I_3, \quad \text{for } Q > 0, \tag{45}$$

$$I_{n,2} = I_1 - I_4, \quad \text{for } Q < 0 \tag{46}$$

and

$$I_{n,2} = -I_3 - I_4, \quad \text{for } Q = 0. \tag{47}$$

The transformed integration contours, which alleviate the oscillatory behavior of the integrand in Equation (23), have been completed in Equations (34)–(36) and (41)–(43). The corresponding integrals have been presented in Equations (37)–(40) and (45)–(47) respectively. All of the integrals derived above can be expressed in a general form as follows:

$$I = \int f(c)\,\mathrm{d}c, \tag{48}$$

where $c = \alpha + i\beta$, as was defined previously. To facilitate the numerical integration, the use of the method of parameter yields

$$I = \int f(\alpha)\left(1 + i\frac{\mathrm{d}\beta}{\mathrm{d}\alpha}\right)\mathrm{d}\alpha. \tag{49}$$

If α is a constant, then

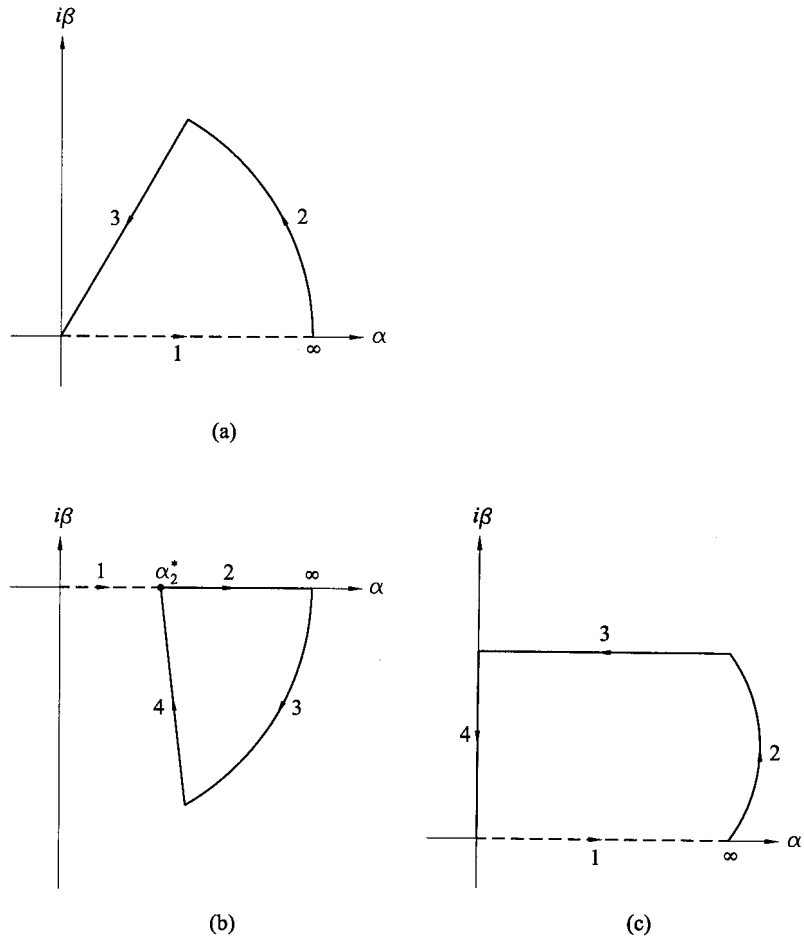

Figure 3. Contour of integration in the complex plane for $I_{n,2}$ with (a) $Q > 0$, (b) $Q < 0$, and (c) $Q = 0$.

$$I = i \int f(\beta)\, \mathrm{d}\beta. \tag{50}$$

By using Equations (49) and (50), the integrals derived earlier can be evaluated numerically.

To illustrate the above transformation method, Figure 4(a) and Figure 5(a) plot the integrands $f_{n,1}(\alpha)$ of Equation (25) and $f_{n,2}(\alpha)$ of Equation (26) respectively for the case $Q > 0$ and selected values of parameters. Figure 4(b) and Figure 5(b) present the corresponding transformed integrands along the paths governed by Equations (34) and (41) respectively. For clarity, dashed lines plot the integration contours. The above figures clearly indicate that the oscillatory behavior is eliminated. Moreover, as α increases, the value $f_{n,1}$ in Figure 4(b) is substantially smaller than that in Figure 4(a) and quickly approaches zero at $\alpha \approx 2$. Notably,

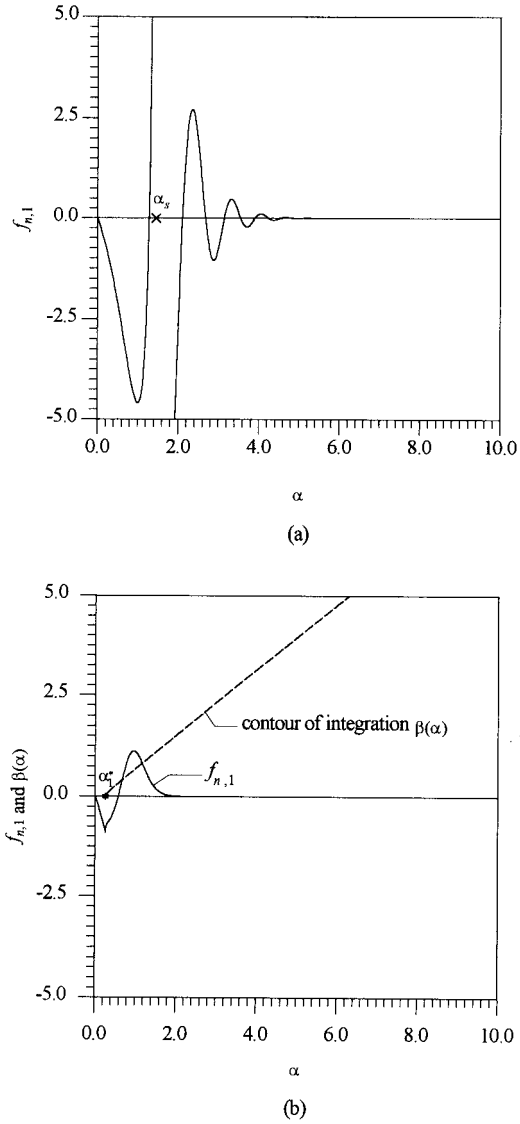

Figure 4. Integrand $f_{n,1}$ of integral $I_{n,1}$ (a) before transformation and (b) after transformation with $T = 0.1$, $u_n = 2.1547$, $x - \xi = 1.0$, $y + \eta = -0.25$, $z - \zeta = 0.25$, and $\theta = 0.0$.

Figure 5(a) and (b) plot the abscissa in different scales. The value $f_{n,2}$ in Figure 5(b) rapidly approaches zero at $\alpha \approx 0.04$. The efficacy of the proposed method used to deal with Equation (2) is then justified. Similarly, the functions $\partial G/\partial n$ and $\partial(\partial G/\partial n)/\partial t$ can also be treated by the proposed technique without difficulty. Further discussion related to those two functions is not intended.

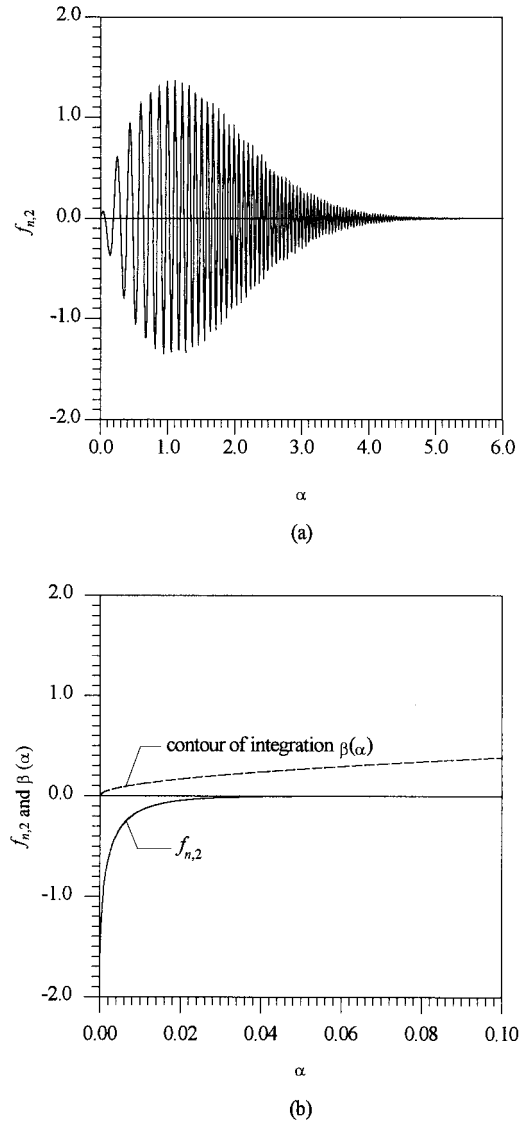

Figure 5. Integrand $f_{n,2}$ of integral $I_{n,2}$ (a) before transformation and (b) after transformation with $T = 6.9614$, $u_n = 2.1547$, $x - \xi = 1.0$, $y + \eta = -0.25$, $z - \zeta = 0.25$, and $\theta = 0.0$.

4. AN INTERPOLATION METHOD FOR EVALUATING MATRIX ELEMENTS

In the framework of IE methods, constructing the related matrices is known to account for the major portion of the computation time. Furthermore, the matrix elements must be recalculated when the system of collocation points is altered. The solution procedure is then not economically feasible at all for the steady problem, and even makes the numerical implementation intractable for the unsteady problem. Without a significant loss of accuracy, an interpolation method is introduced in the following to avoid the type of difficulty. Notably, the integral $F_n(x-\xi, y+\eta, z-\zeta; T)$ in Equation (23) is a function of variables time t and relative positions $x-\xi, y+\eta$ and $z-\zeta$, and not absolute positions x, y, z, ξ, η and ζ separately. Restated, the integral indicates that, in addition to t, only the relative positions of the source points to the field points should be considered. Therefore, databases can be established in terms of parameters $x-\xi, y+\eta$ and $z-\zeta$. For instance, consider a prolate spheroid of major axis $2a$ and minor axis $2b$ under a free surface with submergence depth d. For convenience, the origin of the co-ordinate system is moved from the undisturbed free surface to the body center. All related equations presented previously can be applied by replacing $y+\eta$ with $y+\eta-2d$. A region in terms of these three parameters can then be obtained in the following manner:

$$\begin{aligned} &-2a \le x-\xi \le 2a, \\ &-2b-2d \le y+\eta-2d \le 2b-2d, \\ &0 \le z-\zeta \le 2b. \end{aligned} \tag{51}$$

In the calculations in Section 5, the databases used to evaluate the integral in Equation (2) are established by assigning $a=1.5$ and $b=0.25$, and by a grid system of 31, 11 and 6 collocation points in x, y and z directions respectively with equal spaces. Herein, a quadratic interpolation formula is used to evaluate the values of integral from databases. Figure 6 presents a typical example for selected values of parameters. Comparing the interpolated values with the calculated values obviously reveals the method's accuracy and efficiency. In general, an absolute error of 10^{-5} is obtained in the calculations. The proposed approach is particularly adaptable to the change of the grid system because recalculation for the matrix elements is unnecessary, except for a simple interpolation.

5. NUMERICAL EXAMPLES

Calculations are performed in this paper for a stationary prolate spheroid of co-ordinate surface

$$\frac{x^2}{a^2}+\frac{y^2+z^2}{b^2}=1, \quad a>b, \tag{52}$$

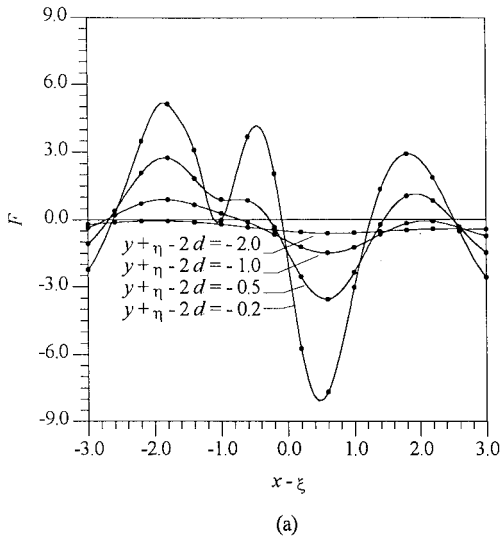

(a)

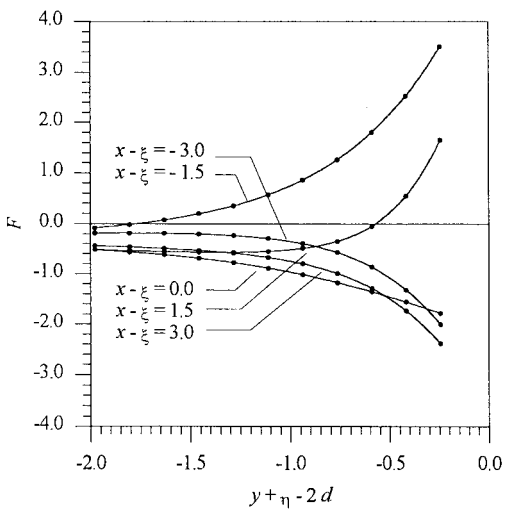

(b)

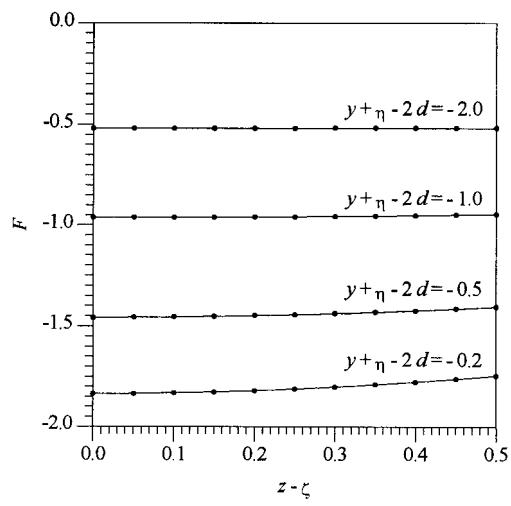

(c)

Figure 6. Comparison of the interpolated values (·) with the calculated values (—) for $F(x-\xi, y+\eta-2d, z-\zeta; T)$ in Equation (23) with $T=0.6961$, $u_n=2.1547$. (a) F versus $x-\zeta$ for $z-\zeta=0$, (b) F versus $y+\eta-2d$ for $z-\zeta=0$, and (c) F versus $z-\zeta$ for $x-\xi=0$.

with submergence depth d in a uniform stream of velocity $-u(t)$ (Figure 7). The Cartesian co-ordinates xyz are related to the spheroidal co-ordinates $\lambda\Omega\Theta$ by

$$x = l \cosh \lambda \cos \Omega,$$

$$y = l \sinh \lambda \sin \Omega \cos \Theta, \tag{53}$$

$$z = l \sinh \lambda \sin \Omega \sin \Theta,$$

where $0 \leq \Omega < \pi$, $0 \leq \Theta \leq 2\pi$ and l denotes the focal distance of the spheroid. First, the non-singular integral Equation (15) used to solve the source function σ is examined for $d \to \infty$. Also adopted herein is a 6-to-1 prolate spheroid. The 30-point Gauss–Legendre quadrature formula is applied along the Ω direction. Meanwhile, the 30-point trapezoidal rule with equal segments, i.e. the most accurate quadrature formula for cyclic integrands [21], is applied along the Θ direction. The method of successive approximations is used to obtain the solution to the system of linear algebraic equations. Notably, the same shape of spheroid, grid system and iteration scheme is employed for the steady and the unsteady problems studied below. To start the numerical iteration process, an initial guess of σ is set at zero and, then, an absolute error of 10^{-5} is reached after 20 iterations. Doubling the integration points yields the results with an accuracy of about the same order and, therefore, verifies the independence of the number of integration points. Figure 8 illustrates the calculated and analytical source strengths against Ω. Comparing the calculated results with the analytical solution demonstrates the effectiveness of the formulation. The corresponding closed-form solution of the source function on the surface of the spheroid, $\lambda = \lambda_0$, is derived in Appendix A and can be written as

$$\sigma = -\frac{u \cos \Omega (\cosh^2 \lambda_0 - 1)^{1/2}}{4\pi(\cosh^2 \lambda_0 - \cos^2 \Omega)^{1/2}} \left(1 - \frac{Q_1(\cosh \lambda_0)}{\cosh \lambda_0 \, \dot{Q}_1(\cosh \lambda_0)}\right), \tag{54}$$

where Q_1 denotes the Legendre function of the second kind of degree one defined by

$$Q_1(\cosh \lambda_0) = \frac{\cosh \lambda_0}{2} \ln \frac{\cosh \lambda_0 + 1}{\cosh \lambda_0 - 1} - 1, \tag{55}$$

and

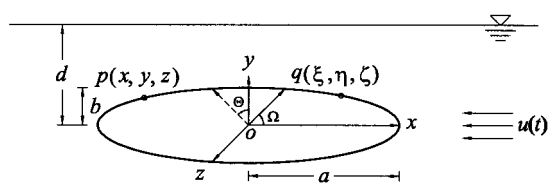

Figure 7. Co-ordinate system of a submerged prolate spheroid.

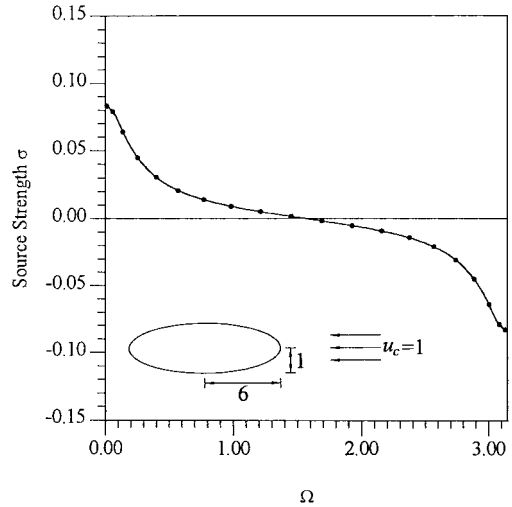

Figure 8. Surface distribution σ of a 6-to-1 spheroid in an unbounded fluid domain (—: analytical solution; ·: calculated value using the proposed method).

$$\dot{Q}_1(\cosh \lambda_0) = \frac{1}{2} \ln \frac{\cosh \lambda_0 + 1}{\cosh \lambda_0 - 1} - \frac{\cosh \lambda_0}{\cosh^2 \lambda_0 - 1}. \tag{56}$$

Next, consider the steady problem, i.e. $-u(t) = -u_c$, which is constant, and $t \to \infty$, for a preliminary examination of the proposed solution method, including the mathematical formulations in Section 2, the technique used to alleviate the oscillatory behavior in Section 3 and the interpolation technique in Section 4. This case makes use of Equation (21). Farell [22] investigated the physical case by expanding the potential function in a power series of spheroidal harmonics. Also studied herein is the surge force F_x, similarly referred to as the wave resistance, because the variation of this quantity is of most interest to engineers. To facilitate physical analysis, let us define the pressure coefficient by $C_P = (P - P_\infty)/(\rho u_c^2/2)$, the wave resistance coefficient by $C_F = F_x/(\pi \rho g l^3)$, and the Froude number by $F_r = u_c/(2gl)^{1/2}$ respectively. Herein, an absolute error of 10^{-5} between two successive approximations for the source function is again reached after about 20 iterations, and the independence of the grid system is examined by doubling integration points. Figure 9 plots the wave resistance coefficient versus the Froude number for three relative submergence depths $d/l = 0.252$, 0.3266 and 0.5 respectively. Havelock's [23] approximation corresponds to the first-order solution of Farell's analysis. The following formula, based on the trapezoidal rule with small segment Δh, is used to evaluate the Cauchy principal value integrals [24]:

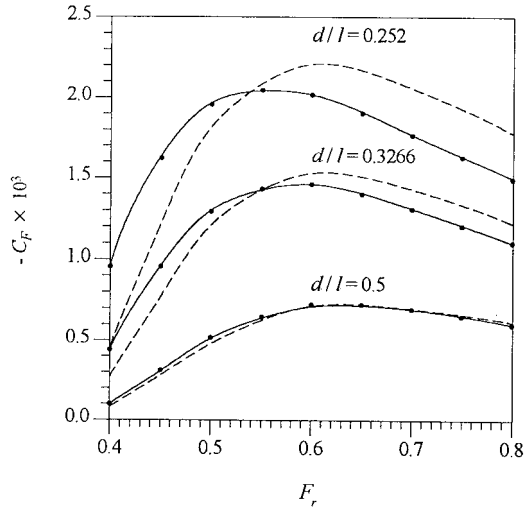

Figure 9. Wave resistance coefficient of a 6-to-1 spheroid (—: Farell's solution; – –: Havelock's solution; ·: calculated value using the proposed method).

$$\text{pr. v.} \int_{a_1}^{a_2} \frac{f(x)}{x - x_0}\,\mathrm{d}x = \frac{\Delta h}{2}\left[\frac{f(a_1)}{a_1 - x_0} + 2\,\frac{f(a_1 + \Delta h)}{a_1 + \Delta h - x_0} + 2\,\frac{f(a_1 + 2\Delta h)}{a_1 + 2\Delta h - x_0} + \cdots + 2\frac{f(x_0 - \Delta h)}{-\Delta h} + 2\,\frac{\mathrm{d}f}{\mathrm{d}x}\bigg|_{x = x_0} + 2\frac{f(x_0 + \Delta h)}{\Delta h} + \cdots + 2\,\frac{f(a_2 - 2\Delta h)}{a_2 - 2\Delta h - x_0} + 2\,\frac{f(a_2 - \Delta h)}{a_2 - \Delta h - x_0} + \frac{f(a_2)}{a_2 - x_0}\right], \tag{57}$$

where $a_1 < x_0 < a_2$. Whenever possible, the term $\mathrm{d}f/\mathrm{d}x$ in the preceding equation is evaluated by a five-point central-difference approximation. As Figure 9 depicts, calculated results using the proposed method correlate well with those of Farell's method. The wave resistance is obviously attributed to the positive hydrodynamic pressure in the front part of the body surface ($0 < \Omega < \pi/2$) and the negative pressure in the rear part ($\pi/2 < \Omega < \pi$). Figure 10 displays the variation of pressure on the body surface by plotting the pressure coefficient C_P against Ω for $d/l = 0.252$ and $F_r = 0.4$, 0.5, 0.6 and 0.7 respectively. According to Figure 10, C_P in the front part of the body negligibly varies with respect to the Froude number. In addition, its value nearly coincides with that of $C_P(\infty)$, which represents a limiting case when $d/l \to \infty$, in the region where $\Omega < 0.3$. Therefore, the pressure in the rear part of the body significantly contributes to the resistance. In the proximity of the body tail, C_P converges to $C_P(\infty)$ with an increase in the Froude number, as indicated in Figure 10. Notably, the negative peak in the rear part gradually moves to the body tail with an increase in the Froude number. Closer examination of Figure 10 indicates that an increase in resistance in Figure 9 for the Froude number increasing from 0.4 to 0.5 is attributed primarily to a decrease in the positive pressure

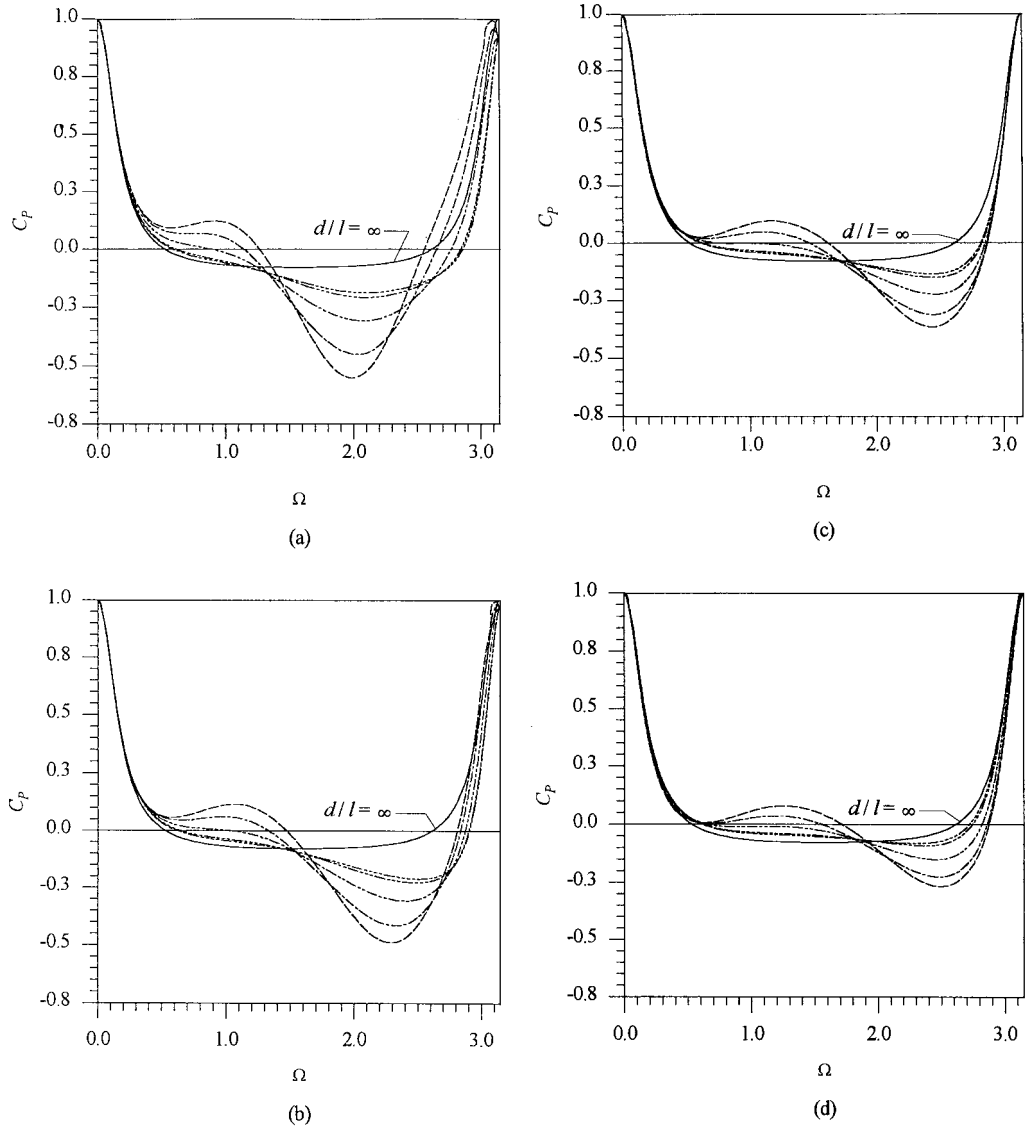

Figure 10. Surface pressure coefficient of a 6-to-1 spheroid for $d/l = 0.252$ and (a) $F_r = 0.4$, (b) $F_r = 0.5$, (c) $F_r = 0.6$, (d) $F_r = 0.7$ (– –: $\Theta = 0.0216$; – - –: $\Theta = 0.7969$; – -- –: $\Theta = 1.5367$; – --- –: $\Theta = 2.4260$; – ---- –: $\Theta = 2.9011$).

in the rear part. In contrast, a decrease in resistance in Figure 9 for the Froude number increasing from 0.6 to 0.7 is attributed to a decrease in absolute values of the negative pressure in the rear part. A balance of the dynamic effects then yields a peak value of resistance at

$F_r \approx 0.55$ for $d/l = 0.252$, as indicated in Figure 9. For $F_r = 0.5$ and $d/l = 0.3266$ and 0.5 respectively, Figure 11 depicts how the submergence depth influences C_P. As is expected, a deeper submergence depth implies a closer pressure distribution to $C_P(\infty)$, which can be written in exact form by

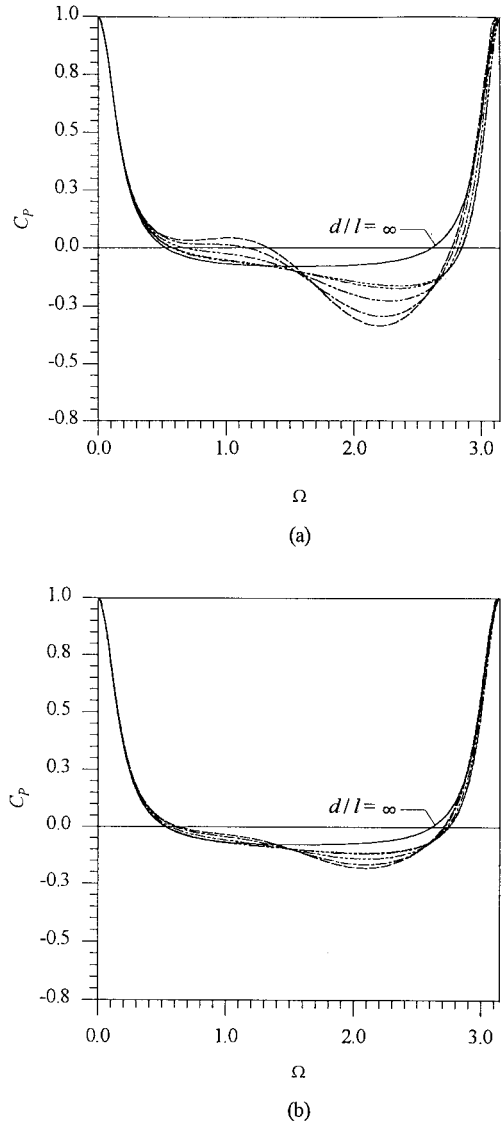

Figure 11. Influence of submergence depth on the pressure coefficient for $F_r = 0.5$ and (a) $d/l = 0.3266$, (b) $d/l = 0.5$ (– –: $\Theta = 0.0216$; – - –: $\Theta = 0.7969$; – -- –: $\Theta = 1.5367$; – --- –: $\Theta = 2.4260$; – ---- –: $\Theta = 2.9011$).

$$C_P(\infty) = 1 - \frac{\sin \Omega}{\cosh^2 \lambda_0 - \cos^2 \Omega} \left[\cosh \lambda_0 - \frac{Q_1(\cosh \lambda_0)}{\dot{Q}_1(\cosh \lambda_0)} \right]^2. \tag{58}$$

Lines with respect to the exact solution (58) and the numerical result are plotted in Figure 10. No clear distinction between them confirms the accuracy of the presented method.

The first unsteady problem is implemented by considering an impulsive start with a constant velocity $-u_c$. In this case, Equation (20) is exploited. Figure 12 displays the resistance coefficient C_F against the dimensionless parameter L/a for $d/l = 0.3$, 0.4 and 0.5 and $F_r = 0.4$ and 0.5 respectively, where L denotes the traveling distance from the starting point. Dashed lines denote the corresponding C_F when $t \to \infty$. Notably, C_F rapidly increases; thereafter, the curves oscillate with a decreasing amplitude around the corresponding limiting values. The appearance of the first peak, which overshoots the limiting value, might be attributed to the inertia effect of the body motion. Figure 12 also reveals that, at the same submergence depth, the amplitude becomes smaller and that, in the meantime, the period becomes longer for the larger Froude number. Notably, the general character of Figure 12 greatly resembles that given by Havelock [3], which presented a first-order approximation of solution for a submerged cylinder started from rest with a constant speed. The second unsteady problem is implemented by considering an impulsive start with a constant acceleration $\dot{u}(t)$ up to a final constant speed. Figure 13 displays the resistance coefficient C_F against the dimensionless parameter L/a for $d/l = 0.5$. Also plotted in Figure 13 is the velocity $u(t)$ against L/a. The corresponding Froude number of the final speed takes the value 0.4, and the dashed line indicates the limiting case when $t \to \infty$. In this case, the variation of C_F at the incipient stage is of priority concern. In general, a similar oscillating and decaying behavior as in the previous case is observed. As Figure 13 indicates, the sudden decrease in C_F at $L/a = 5.5$ is attributed to the disappearance of the impulsive acceleration. Then C_F increases to its maximum value at $L/a = 8.5$. The memory effect preserves this wavy-peak pattern at each period as L/a increases. The oscillating behavior is a result of the hydrodynamic interactions of the free surface and the body, i.e. the time variation of pressure on the body surface. The memory effect also indicates that each case in Figures 12 and 13 remains its own particular wave pattern as in the incipient stage with the amplitude reduced gradually with respect to time. At a small value of time $t = 0.01$, the calculated value of the resistance coefficient $C_F = -4.5 \times 10^{-5}$ is extremely close to that of the resistance coefficient $C_F^* = -4.8 \times 10^{-5}$. Notably, the resistance coefficient C_F^* is defined by $C_F^* = -m\dot{u}(t)/(\pi \rho g l^3)$, where m denotes the corresponding added-mass coefficient of the spheroid in an unbounded fluid domain. The above finding confirms the physical intuition that the hydrodynamic force acting on an impulsively accelerating body under a free surface at $t \to 0^+$ is equivalent to the force acting on the body without other boundaries. The added-mass coefficient,

$$m = \frac{l^2}{a^2 - \dfrac{ab^2}{2l} \ln \dfrac{a+l}{a-l}} - 1, \tag{59}$$

is derived in Appendix A using the Taylor theorem [25]. All computations presented above are performed on a HP-Apollo 730 workstation. For the steady problem, each value of wave

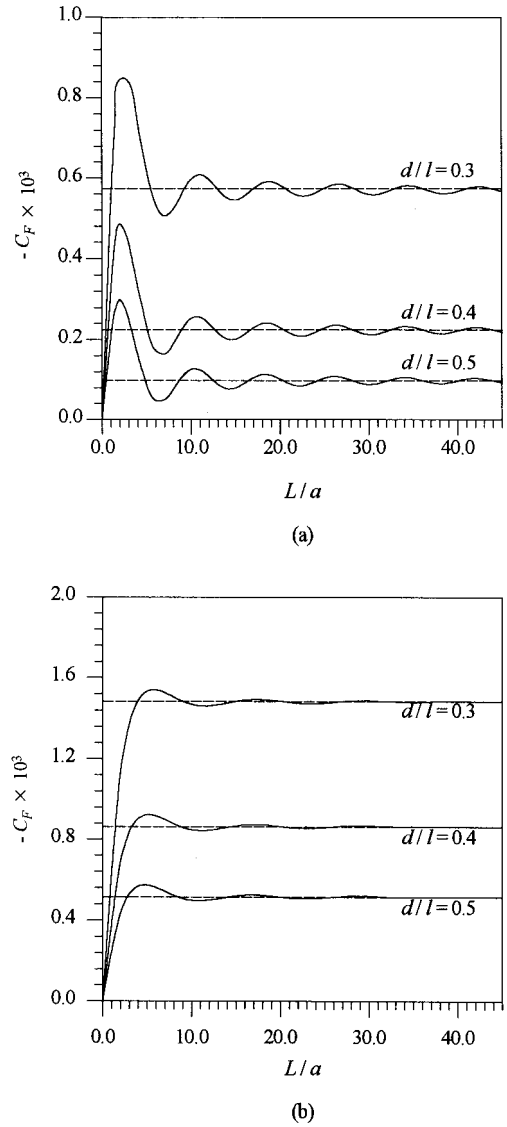

Figure 12. Wave resistance coefficient for an impulsive start with a constant velocity and (a) $F_r = 0.4$, (b) $F_r = 0.5$.

resistance coefficient takes about 1 min of central processing unit (CPU) time. For the case of an impulsive start with a constant velocity, each case (given a Froude number and a submergence depth) with 23 time steps takes about 25 min.

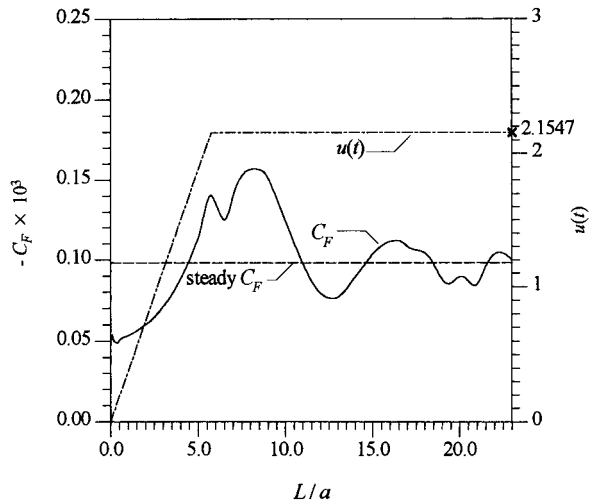

Figure 13. Wave resistance coefficient for an impulsive start with a constant acceleration and $d/l = 0.5$.

6. CONCLUDING REMARKS

This paper presents an effective solution method to evaluate the hydrodynamic forces of translating bodies under a free surface. The proposed method is implemented in the following manner: (1) the non-singular integral equation formulations, which are amenable to the solution by directly using quadrature formulas; (2) the transformed integration contours, thereby averting the difficulty in evaluating highly oscillatory integrals; and (3) the interpolation scheme, which is used to assess the matrix elements and is particularly adaptable to the change of the grid system. The efficiency of the proposed desingularization scheme has been examined by Yang [26] by considering the potential flow of an ellipse translating in an unbounded fluid domain. Numerical results indicate that the proposed scheme is more economic and accurate than the flat-element constant-source boundary element (BE) method. For instance, the CPU time of the proposed scheme is about half of that of the BE method for 50 collocation points, and about a quarter of that for 200 collocation points. Meanwhile, the accuracy of relative error is improved by at least one order of 10^{-1}.

Numerical calculations are performed for a prolate spheroid in a uniform flow parallel with the major axis. The proposed method's effectiveness is confirmed by comparing the calculations with the analytical solution when a free surface is not present, and with the closed-form series solution when a free surface is present and time t approaches infinity. For the latter case, the variation of wave resistance against the Froude number is studied in detail. In general, the proposed numerical method successfully removes the limitations of asymptotic analyses. The latter methods yield solutions available for large time or small time only, as is mentioned in Section 1.

The proposed method can be extended to more general body configurations under more complicated circumstances by incorporating the BE methods. From a numerical perspective, the surface-discretization formulation used herein is a local method. In general, the methods divide the integration domain into small elements, and the unknown functions are defined as piecewise polynomial functions of a fixed degree on the elements of the subdivision. In contrast, when the unknown functions in the integral equations are globally defined, in some sense, as smooth functions on the integration domain, the numerical methods are generally referred to as global methods. Most of the numerical methods used to solve boundary integral equations in the engineering literature have been local methods. They are also referred to as BE methods. BE methods flexibly handle a variety of surfaces, boundary conditions, and changes in the smoothness of the unknown density function. For smooth body surfaces, the global methods can be much more efficient with respect to computation time and storage, when compared with the BE methods [27]. Therefore, in a future study, we recommend incorporating a proper global method into the proposed solution method.

One possible future study includes comparing the presented numerical results with experimental data. Conducting the related experiments in the towing tank is extremely difficult; this difficulty is ascribed to a problem of accurately controlling a pre-assigned, unsteady speed of the carriage, i.e. the repeatability problem. Another problem is the dynamic effects on the entire measuring system, including the dynamic calibrations (in contrast with the static ones) of the measuring instruments, e.g. the force or pressure transducers [28,29]. Another future study includes the problems of an airfoil or spheroid moving at a different angle of attack. The unsteady Kutta condition must be considered at the trailing edge. The time variation of induced vortices is of greatest interest in this case.

Finally, it is worth noting that this work exploits the Bernoulli equation, which expresses the forces by integrating the pressure over the body surface. Other approaches could be applied to the title problem. The first concerns Lagrange's equation of motion, which expresses the forces in terms of added masses and their derivatives [30,31]. Taylor's formula is then deemed necessary to evaluate added masses [25,32]. The second approch concerns the Lagally theorem, which expresses the dynamic effects in terms of singularities and gradients of velocity potential [33,34]. Although all results can presumably be obtained equally well by these three methods for the current problem, the proposed method appears to be more straightforward in mathematical formulation and easier in numerical implementation.

ACKNOWLEDGMENTS

The author would like to thank the National Science Council, R.O.C. for financially supporting this research under contract no. NSC 84-2611-E-006-020 and C.C. Chieu for his programming assistance.

APPENDIX A. EXACT SOLUTIONS OF THE SURFACE SOURCE FUNCTION AND ADDED MASS OF A PROLATE SPHEROID IN A UNIFORM STREAM

Consider a stationary prolate spheroid of co-ordinate surface,

$$\frac{x^2}{a^2}+\frac{y^2+z^2}{b^2}=1, \quad a>b, \tag{A1}$$

in a uniform stream of constant velocity u in the positive x direction. The spheroidal co-ordinates $\lambda\Omega\Theta$ are related to the Cartesian co-ordinates xyz by

$$x = l\cosh\lambda\cos\Omega = l\gamma\mu,$$

$$y = l\sinh\lambda\sin\Omega\cos\Theta = l(\gamma^2-1)^{1/2}(1-\mu^2)^{1/2}\cos\Theta \tag{A2}$$

and

$$z = l\sinh\lambda\sin\Omega\sin\Theta = l(\gamma^2-1)^{1/2}(1-\mu^2)^{1/2}\sin\Theta,$$

where $\gamma=\cosh\lambda$, $\mu=\cos\Omega$, $\gamma\geq 1$ and $\mu\leq 1$. The velocity potential exterior to the spheroid can be written as [35]

$$\phi_E = ul\gamma\mu + \sum_{k=0}^{\infty}\sum_{s=0}^{k} P_k^s(\mu)Q_k^s(\gamma)[A_{1k}^s\cos(s\Theta)+A_{2k}^s\sin(s\Theta)], \tag{A3}$$

where A_{1k}^s and A_{2k}^s are the coefficients to be determined. The associated Legendre's functions are defined by

$$P_k^s(\mu) = (1-\mu^2)^{s/2}\frac{\mathrm{d}^s P_k(\mu)}{\mathrm{d}\mu^s}, \tag{A4}$$

$$P_k^s(\gamma) = (\gamma^2-1)^{s/2}\frac{\mathrm{d}^s P_k(\gamma)}{\mathrm{d}\gamma^s} \tag{A5}$$

and

$$Q_k^s(\gamma) = (\gamma^2-1)^{s/2}\frac{\mathrm{d}^s Q_k(\gamma)}{\mathrm{d}\gamma^s}. \tag{A6}$$

Notably, $Q_k^s(\mu)$ is omitted in Equation (A3) for the finiteness condition. From the boundary condition,

$$\left.\frac{\partial\phi_E}{\partial n}\right|_{\gamma=\gamma_0} = 0, \tag{A7}$$

A_{1k}^s and A_{2k}^s are obtained and Equation (A3) reduces to

$$\phi_E = ul\mu\left[\gamma - \frac{Q_1(\gamma)}{\dot{Q}_1(\gamma_0)}\right], \tag{A8}$$

where

$$\dot{Q}_1(\gamma_0) = \frac{1}{2}\ln\frac{\gamma_0+1}{\gamma_0-1} - \frac{\gamma_0}{\gamma_0^2-1}. \tag{A9}$$

The corresponding interior velocity potential can be written as

$$\phi_I = ul\gamma\mu + \sum_{k=0}^{\infty}\sum_{s=0}^{k} P_k^s(\mu)P_k^s(\gamma)(B_{1k}^s\cos s\Theta + B_{2k}^s\sin s\Theta), \tag{A10}$$

where B_{1k}^s and B_{2k}^s are the coefficients to be determined. Applying the continuity condition of the velocity potential at the boundary, i.e. $\phi_E = \phi_I$, yields

$$\phi_I = ul\mu\gamma\left[1 - \frac{Q_1(\gamma_0)}{\gamma_0\dot{Q}_1(\gamma_0)}\right], \tag{A11}$$

where

$$Q_1(\gamma_0) = \frac{\gamma_0}{2}\ln\frac{\gamma_0+1}{\gamma_0-1} - 1. \tag{A12}$$

By making use of the jump condition,

$$\sigma = \frac{1}{4\pi}\left(\frac{\phi_E}{n} - \frac{\phi_I}{n}\right)_{\gamma=\gamma_0} = -\frac{1}{4\pi}\left(\frac{\phi_I}{n}\right)_{\gamma=\gamma_0}, \tag{A13}$$

the surface source function can be obtained in the following equation:

$$\sigma = -\frac{u\mu(\gamma_0^2-1)^{1/2}}{4\pi(\gamma_0^2-\mu^2)^{1/2}}\left(1 - \frac{Q_1(\gamma_0)}{\gamma_0\dot{Q}_1(\gamma_0)}\right). \tag{A14}$$

By making use of Taylor's formula, the added mass can be written as follows:

$$M = -\frac{4\pi\rho ab^2}{3} + 4\pi\rho\int\sigma x\,\mathrm{d}S, \tag{A15}$$

where $\mathrm{d}S = l^2(\cosh^2\lambda_0 - \cos^2\Omega)^{1/2}\sinh\lambda_0\sin\Omega\,\mathrm{d}\Omega\,\mathrm{d}\Theta$. The added-mass coefficient is defined by

$$m = \frac{M}{\frac{4}{3}\pi\rho ab^2} = \frac{l^2}{a^2 - \frac{ab^2}{2l}\ln\frac{a+l}{a-l}} - 1. \tag{A16}$$

REFERENCES

1. J.K. Lunde, 'On the linearized theory of wave resistance for displacement ships in steady and accelerated motion', *Trans. SNAME*, **59**, 25–76 (1951).
2. L.N. Sretenskii, 'On the theory of wave resistance', *Trudy Tsentral Aero-Gidrodinam. Inst. vyp.*, vol. 348, 1939 (in Russian).
3. T.H. Havelock, 'The wave resistance of a cylinder started from rest', *Q. J. Mech. Appl. Math.*, **2**, 325–334 (1949).
4. T.H. Havelock, 'The resistance of a submerged cylinder in accelerated motion', *Q. J. Mech. Appl. Math.*, **2**, 419–427 (1949).
5. J.V. Wehausen, 'Effect of the initial acceleration upon the wave resistance of ship models', *J. Ship Res.*, **7**, 38–50 (1964).
6. A.N. Shebalov, 'Theory of wave resistance of a ship in unsteady motion on calm water', *Tr. Leningr. Korablestroi. Inst.*, **52**, 209–220 (1966) (in Russian).
7. Y. Liu and D.K.P. Yue, 'On the time dependence of the wave resistance of a body accelerating from rest', *J. Fluid Mech.*, **310**, 337–363 (1996).
8. A.M.O. Smith, J.P. Giesing and J.L. Hess, 'Calculation of waves and wave resistance for bodies moving on or beneath the surface of the sea', *Report No. 31488A*, Aircraft Division, Douglas Aircraft Company, Long Beach, CA, 1963.
9. H.-T. Shen and C. Farell, 'Numerical calculation of the wave integrals in the linearized theory of water waves', *J. Ship Res.*, **21**, 1–10 (1977).
10. J.N. Newman, 'Evaluation of the wave-resistance Green function: part 1—the double integral', *J. Ship Res.*, **31**, 79–90 (1987).
11. Q. Huang and T.A. Cruse, 'Some notes on singular integral techniques in boundary element analysis', *Int. J. Numer. Meth. Eng.*, **36**, 2643–2659 (1993).
12. L. Landweber and M. Macagno, 'Irrotational flow about ship forms', *IIHR Report No.123*, Iowa Institute of Hydraulic Research, The University of Iowa, Iowa City, IA, 1969.
13. N.M. Günter, *Potential Theory and Its Applications to Basic Problems of Mathematical Physics*, Ungar, New York, 1967, p. 1.
14. W. Pogorzelski, *Integral Equations and Their Applications*, Pergamon, Oxford, 1966, pp. 230–339.
15. O.D. Kellogg, *Foundations of Potential Theory*, Springer, Berlin, 1929.
16. N.I. Muskhelishvili, *Singular Integral Equations*, Noordhoff, Groningen, 1953.
17. S.G. Mikhlin, *Integral Equations*, Pergamon, London, 1957.
18. L.N.G. Filon, 'On a quadrature formula for trigonometric integrals', *Proc. R. Soc. Edinburgh*, **49**, 38–47 (1928).
19. R. Piessens and F. Poleunis, 'A numerical method for the integration of oscillatory functions', *BIT*, **11**, 317–327 (1971).
20. A. Alaylioglu, G.A. Evans and J. Hyslop, 'The use of Chebyshev series for the evaluation of oscillatory integrals', *Comput. J.*, **19**, 258–267 (1976).
21. K.E. Atkinson, *An Introduction to Numerical Analysis*, Wiley, New York, 1988, pp. 249–329.
22. C. Farell, 'On the wave resistance of a submerged spheroid', *J. Ship Res.*, **17**, 1–11 (1973).
23. T.H. Havelock, 'The wave resistance of a spheroid', *Proc. R. Soc. London Ser. A*, **131**, 275–285 (1931).
24. H.E. Kobus, 'Examination of Eggers' relationship between transverse wave profiles and wave resistance', *J. Ship Res.*, **11**, 240–256 (1967).
25. G.I. Taylor, 'The energy of a body moving in an infinite fluid, with an application to airships', *Proc. R. Soc. London Ser. A*, **120**, 13–21 (1928).
26. S.A. Yang, 'A solution method for two-dimensional potential flow about bodies with smooth surfaces by direct use of the boundary integral equation', *Commun. Numer. Method Eng.*, **15**, 469–478 (1999).
27. K.E. Atkinson, 'A survey of boundary integral equation methods for the numerical solution of Laplace's equation in three dimensions', in M.A. Golberg (ed.), *Numerical Solution of Integral Equations*, Plenum Press, New York, 1990.
28. M.D. Pearlman, 'Dynamic calibration of wave probes', *M.I.T. Contract No. DSR 6913*, Department of Naval Architecture and Marine Eng., Massachusetts Institute of Technology, 1963.
29. K.H. Wang and A.T. Chwang, 'Free-surface flow produced by an accelerating vertical cylinder', *J. Eng. Mech.*, **115**, 1559–1566 (1989).
30. H. Lamb, *Hydrodynamics*, Dover, New York, 1932, pp. 160–201.
31. G.A. Athanassoulis and T.A. Loukakis, 'Lagrangian expressions of the hydrodynamic forces acting on a rigid body in the presence of a free surface', *J. Ship Res.*, **29**, 12–22 (1985).
32. L. Landweber, 'On a generalization of Taylor's virtual mass relation for Rankine bodies', *Q. Appl. Math.*, **14**, 51–56 (1956).
33. W.E. Cummins, 'The forces and moments acting on a body moving in an arbitrary potential stream', *Report No. 708*, *David Taylor Model Basin*, 1953.
34. L. Landweber and C.S. Yih, 'Forces, moments, and added masses for Rankine bodies', *J. Fluid Mech.*, **1**, 319–336 (1956).
35. P. Moon and D.E. Spencer, *Field Theory Handbook*, Springer, Berlin, 1988.

